BIOCHE 01792

Fluorescence lifetime imaging microscopy (FLIM): Spatial resolution of microstructures on the nanosecond time scale

Theodorus W.J. Gadella, Jr., Thomas M. Jovin and Robert M. Clegg *

Department of Molecular Biology, Max Planck Institute for Biophysical Chemistry, Postfach 2841, D-37018 Göttingen (FRG)

Abstract

A frequency domain fluorescence lifetime imaging microscope (FLIM) has been developed. A continuous wave laser excitation source of an epi-illumination fluorescence microscope is modulated at a high frequency f_A. The lifetime of the modulated fluorescence emission is determined from the phase delay and modulation depth of the fluorescence signal relative to that of the excitation light. Phase detection is accomplished simultaneously at every location in the image by modulating the high voltage amplification stage of a microchannel plate image intensifier at a frequency near (heterodyne method) or at (homodyne method) f_A. The heterodyne or homodyne image output of the intensifier is focused onto a cooled high resolution charge-coupled-device camera for digital recording and subsequent analysis of phase and modulation. The technique has the sensitivity of normal steady state microscopy, and is relatively simple to employ. We present several examples illustrating the applications of FLIM for determining prompt fluorescence lifetimes in picoliter homogeneous solutions, for lifetime imaging of single cells, and for phase suppressing particular lifetime components in fluorescence images. Several unique aspects of lifetime resolved image processing are featured and discussed, including the analysis, statistical evaluation, and display of the data. Coupling of the spatial and temporal aspects of fluorescence images extends considerably the possibilities for quantitative fluorescence microscopy.

1. Introduction

Fluorescence microscopy applied to biological samples has been evolving rapidly due to dramatic technological advances in image generation and detection, and in the performance of the associated computers [1]. New luminescent probes for visualizing cellular components have provided the specificity required by the cell biologist [2–7], while image detectors, especially cameras based on charge-coupled devices (CCDs) [8] and image intensifiers [9], offer the corresponding sensitivity, spectral response, background suppression and speed. In addition, improvements in the design of optical microscopes have significantly in-

---

* Corresponding author. Fax (+49-551) 201-467.

creased the efficiency of light transmission and the spectral range for excitation and detection, as exemplified in "multi-mode" instruments [9–12]. It remains a challenge, however, to implement systematically in the microscope all the photophysical modalities that are currently available in "cuvette" systems.

Novel optical parameters, such as fluorescence anisotropy [13–16], dichroism [17–20], and fluorescence resonance energy transfer [21, 22] have been incorporated into microscope systems. However, almost all the parameters based on fluorescence have involved the measurement of steady state signals. They have not, in general, exploited the statistical nature and temporal decay laws of light emission from the excited states of fluorophores. As a consequence, the intrinsic information provided by the fluorescence lifetimes about the dynamic properties and the chemical and physical environments of the various species has not been available.

Fluorescence lifetimes are sensitive indicators of local pH and ionic activity, the influence of quencher molecules and energy-transfer acceptors, and the state of ligand binding or macromolecular association. These biochemical and biophysical quantities have been featured prominently over the last 20 years of time-resolved fluorescence spectroscopy carried out with macroscopic amounts of samples in cuvettes [23–25] (see also accompanying papers in this issue). Corresponding studies in the microscope have been more limited. The initial measurements had poor spatial resolution due to the acquisition of data from relatively large sample areas using either single photon detection techniques based on photomultipliers [14,26,27] or frequency domain methods [28,29].

Only recently has it become possible to correlate time dependent photophysical and chemical information with the spatial distributions of structures and molecules in a microscope image. We have previously denoted this technique as time-resolved imaging microscopy (TRIM) [29] but adopt here the designation FLIM (fluorescence lifetime imaging microscopy) to be compatible with other designations [30]. The requirement is to make measurements of the luminescence de-

cay simultaneously at many pixels of an image, thereby adding a new dimension to cellular imaging. Of central importance in the development of nanosecond lifetime imaging has been the possibility of gating (100% on/off gain control) or continuously modulating the gain of microchannel plate (MCP) image intensifiers. As we demonstrate below, the output of the modulated MCP intensifiers can be conveniently coupled to CCD cameras with high sensitivity and dynamic range in order to acquire lifetime-resolved fluorescence images.

In the "pulse" method for FLIM, the specimen is excited with a short pulse of light and the ensuing fluorescence (or longer-lived) emission is integrated with a gated image intensifier within an adjustable time window [30–35]. This method has been applied in studies based on phosphorescence (time scale ms–s) [32,35,36] and fluorescence [37]. However, the pulse technique has distinct disadvantages in measurements of prompt fluorescence, because most lifetimes are < 5 ns, comparable to the minimal gate widths of most commercial gated image intensifiers [34]. Thus, for fast decaying probes, the temporal resolution and/or signal-to-noise ratio (SNR) may be unacceptably low. In addition, if a mathematical deconvolution is necessary for fitting exponential decays on a pixel-by-pixel basis, exceptionally long computation times are required.

The frequency-domain counterpart for determining prompt fluorescence lifetimes on a pixel-by-pixel basis offers distinct advantages and avoids many of the problems associated with the direct time-domain measurements. The method is under development in a number of laboratories [28,38–45] including our own ([29], R.M. Clegg et al., in preparation; T.W.J. Gadella, Jr. et al., in preparation). We have demonstrated previously the features and applications of a newly developed phosphorescence microscope with a temporal resolution of luminescence decay from 50 μs to many seconds and with digital image acquisition [32]. In this article we describe the development of a lifetime-resolved fluorescence microscope operating in the nanosecond time domain. We discuss the techniques for data acquisition and analysis, emphasizing the particular merits of

FLIM, and illustrate its application with several model and biological systems.

2. Description of the phase and modulation measurements

2.1. General expressions representing the frequency response of a repetitively excited fluorescent sample

The alternative to the pulse method for determining fluorescence lifetimes is to measure the frequency dispersion of the emission during continuous repetitive excitation with modulated light [46–48]. We adopted this technique for implementation in the microscope because of SNR (signal-to-noise ratio) and duty cycle considerations, and the technical capability of acquiring data for very short lifetimes.

If the excitation light $E_\omega(t)$ impinging on a sample is modulated sinusoidally with a frequency f_A (eq. 1), the total emitted (or scattered) light $F_\omega(t)$ emanating from every position of the illuminated object also varies sinusoidally and with the same frequency (eq. 2), regardless of the number of individual lifetime components.

$$E_\omega(t) = E_{0,\omega}\left[1 + M_{E,\omega} \sin(\omega t - \Phi_{E,\omega})\right] \quad (1)$$

$$F_\omega(t) = F_{0,\omega}\left[1 + M_{F,\omega} \sin(\omega t - \Phi_{F,\omega})\right] \quad (2)$$

where $E_{0,\omega}$ is the time invariant (DC) excitation light intensity; $M_{E,\omega}$ is the relative modulation of the excitation light, defined as the amplitude of the time dependent signal $(E_{t,\omega})$ divided by the static DC component $(M_{E,\omega} \equiv E_{t,\omega}/E_{0,\omega})$; the radial frequency $\omega = 2\pi f_A$; $F_{0,\omega}$ is the time invariant total fluorescence emission; $M_{F,\omega}$ is the relative modulation of the total fluorescence emission; and $\Phi_{E,\omega}$ and $\Phi_{F,\omega}$ are the total phase lags of the excitation and the fluorescence emission relative to an arbitrary zero phase set by the electronics. The total phase lag of the fluorescence emission relative to the excitation light $(\Delta\Phi$; range: $0-\pi/2$, for no excited state reactions) and the normalized modulation $(M \equiv M_{F,\omega}/M_{E,\omega}$, range: $0-1)$ are related to the number of contributing fluorescent components (K).

$$\Delta\Phi \equiv \Phi_{F,\omega} - \Phi_{E,\omega}$$
$$= \tan^{-1}\left(\sum_k^K \frac{\alpha_k \omega \tau_k}{1 + (\omega\tau_k)^2} \middle/ \sum_k^K \frac{\alpha_k}{1 + (\omega\tau_k)^2}\right)$$
$$(3a)$$

$$M \equiv \frac{M_{F,\omega}}{M_{E,\omega}} = \left(\left(\sum_k^K \frac{\alpha_k \omega \tau_k}{1 + (\omega\tau_k)^2}\right)^2\right.$$
$$\left. + \left(\sum_k^K \frac{\alpha_k}{1 + (\omega\tau_k)^2}\right)^2\right)^{1/2} \quad (3b)$$

where α_k is the fractional contribution to the steady state fluorescence made by the kth emitting species (with fluorescence lifetime τ_k) under constant illumination conditions; α_k is proportional to $a_k\tau_k$, where a_k is the relative amplitude of the kth exponentially decaying component in the time domain. The emission of molecules with lifetimes for which $\omega\tau_k \approx 1$ contribute most to the demodulation and phase delay of the measured fluorescence signal.

The phase difference $(\Delta\Phi)$ and normalized modulation (M) of the measured signal are the sole information available for determining the luminescence lifetime at each pixel. If these quantities are measured at many different modulation frequencies, the fluorescence lifetimes and the relative amplitudes of several fluorescence components can be determined by fitting the experimental data to the dispersion eqs. (3a,b) [48]. These are the usual procedure and goal of a single channel experiment using a photomultiplier (PM) as the light detector [49]. In principle the same procedure that is applied to PM measurements can be carried out with image devices capable of functioning as phase sensitive detectors for every position in the field. The implementation of this principle in our laboratory is described in the following sections.

2.2. Heterodyne and homodyne methods

By modulating the gain of a MCP intensifier (see Section 3.2) at a frequency that is either

close to (heterodyne method) or the same (homodyne method) as the modulation frequency of the excitation light, $\Phi_{F,\omega}$ and $M_{F,\omega}$ (or $\Phi_{E,\omega}$ and $M_{E,\omega}$; eq. 2) can be analyzed simultaneously at every position of the image generated at the output phosphor screen of the intensifier (see below). Subjecting the high frequency (HF) optical signal (with frequency f_A) to an HF electronic gain modulation (with frequency f_M) in the image intensifier, produces a low frequency sinusoidal modulation of the MCP output at each channel, at the difference frequency $\Delta f = |f_A - f_M|$. In homodyne operation, $\Delta f = 0$ and the measured steady state fluorescence intensity depends only on the phase difference between the two HF signals. In heterodyne operation, $\Delta f \ll f_A$ or f_M, and one measures the intensity and phase of the low frequency signal. These methods of signal detection and analysis are commonly applied to the measurement of fluorescence lifetimes of discrete samples, and have been described extensively in the literature [46,48]. The heterodyne technique offers the advantage that the manipulations of the detected signals are carried out conveniently and accurately at a very low difference frequency (Δf), but the phase and modulation information of the HF fluorescence signal is retained. The lifetime of an unknown compound is extracted after calibrating the system with a reference compound of known lifetime τ_R (eq. 4). The low frequency representation of the unknown sample is given in eq. (5); eqs. (6a,b) redefine the parameters of eqs. (3a,b) in terms of the low frequency phase and modulation components.

$$R_{\Delta\omega}(t) = R_{0,\Delta\omega}[1 + M_{R,\Delta\omega}\sin(\Delta\omega t - \Phi_{R,\Delta\omega})]$$
(4)

$$F_{\Delta\omega}(t) = F_{0,\Delta\omega}[1 + M_{F,\Delta\omega}\sin(\Delta\omega t - \Phi_{F,\Delta\omega})]$$
(5)

$$\Delta\Phi = \Phi_{F,\Delta\omega} - \Phi_{R,\Delta\omega} + \tan^{-1}(\omega\tau_R)$$
$$= \Phi_{F,\Delta\omega} - \Phi_{S,\Delta\omega}$$
(6a)

$$M = \frac{M_{F,\Delta\omega}}{M_{R,\Delta\omega}\sqrt{1 + (\omega\tau_R)^2}} = \frac{M_{F,\Delta\omega}}{M_{S,\Delta\omega}}$$
(6b)

The symbols in eqs. (4) and (5) are analogous to those in eqs. (1) and (2). Note that in eqs. (6a,b), explicit reference is made to the high modulation frequency $\omega = 2\pi f_A$, whereas eqs. (4) and (5) are formulated in terms of the low difference frequency $\Delta\omega = 2\pi\Delta f_A$. The subscript 'S' denotes scattered light as the reference, for which the effective lifetime $\tau_R = 0$. At present, it is impractical to implement the same phase sensitive techniques that are employed in the usual single channel measurement to every pixel of a sensitive image detector. Other methods are required. We describe below the heterodyne-boxcar technique used to acquire the data presented in this paper.

3. Experimental realization of the phase-modulation measurement with an imaging detector

3.1. The fluorescence lifetime microscope

Any fluorescence microscope can be used. The system described here was installed on an epi-illumination Zeiss Universal Microscope (Oberkochen, FRG). Figure 1 shows a block diagram of the microscope and MCP intensifier-CCD detection system. A line selected from a Spectra Physics 2035 argon-ion laser is modulated with acousto-optical modulators (AOMs, IntraAction Corp., Belwood, IL) [49]. The central (or a higher order) spot of the diffraction pattern is focused onto a quartz optical fiber (0.2 mm diameter, several meters in length). The light emitted from
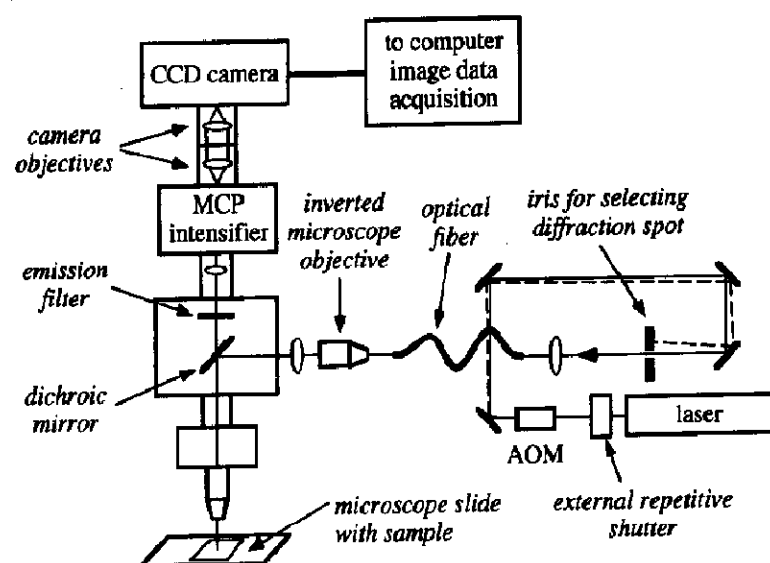

Fig. 1. Fluorescence lifetime imaging microscope. For details see text.

the end of the fiber is directed through an inverted microscope objective and a low power lens into the side entrance of the microscope epi-illumination port. To reduce laser speckle, the optical fiber is vibrated or a highly scattering solution is inserted in the light path. The fluorescence image is focused onto the cathode of the MCP image intensifier. The MCP is attached to the vertical port of the microscope and its output phosphor is imaged through a tandem array of camera objectives to a high dynamic range slow-scan CCD camera. We use a Photometrics (Tucson, Az) series 200 camera system incorporating: (i) a mechanical shutter; (ii) a thermoelectrically cooled CSF-Thomson 7882(1)A CCD sensor with a Metachrome II down converter coating to boost the blue sensitivity, and a 576×384 array of 23×23 μm square pixels, each with a full well capacity of 3.5×10^5 electrons and a dark current of 8 electrons s^{-1}; (iii) a readout noise of 6 electrons; (iv) a 14-bit 50 kHz double correlated analog-to-digital converter; and (v) a camera controller and image storage and display unit with communication to a Apple Macintosh IIci computer with a GPIB interface (National Instruments, NB-DMA-8-G) for recording and processing the digital images. The instrument and user interfaces are implemented with LabView (National Instruments).

The MCP intensifier is part of an "image relay optics" (IRO) system (PCO Computer Optics GmbH, Kelheim, FRG), with pulse controller, S20 photocathode, P46 phosphor, and ~ 5 ns minimum gate. The intensifier has been modified for high frequency (HF) modulation directly at the MCP of the intensifier. The HF driving current is capacitively coupled into the MCP from a power amplifier (Electronic Navigation Instruments, 403LA, 3 watts) driven by a precision HF signal generator (Marconi Instruments, 2022A). All frequency generators are phase locked to a single crystal.

3.2. Gain modulation of the MCP intensifier and measurement of the phase and modulation of the heterodyne difference signal

MCP image intensifiers have been developed with cathodes that can be gated on (or off) within

~ 5 ns, a response sufficiently fast for use in the measurement of nanosecond fluorescence lifetimes [8]. It is also possible to modulate the cathode of a MCP intensifier continuously in the high frequency range compatible with fluorescence lifetimes [38,39]. We have found it more convenient to modulate the intensifier directly at the high voltage amplification stage [29]. This approach, which to our knowledge is unique, offers numerous advantages: (i) absence of channel crosstalk; (ii) uniform modulation over the field (no defocusing from iris effects); (iii) significant depth of modulation (25–35%) sufficient for making accurate pixel-by-pixel phase measurements; and (iv) retention of the cathode for gating.

3.3. Experimental procedure

Figure 2 illustrates the operation of the modulation scheme. The HF frequency of the light and intensifier modulation (25–80 MHz) differ by a small frequency Δf (usually 1 to 1000 Hz). The intensity at the output of each channel i of the MCP is modulated at the frequency Δf, with a phase $\Delta \Phi_i$ and a modulation M_i according to eqs. (6a,b). The heterodyne signal is recorded simultaneously at each pixel of the CCD camera only during a particular phase and fraction of each Δf cycle by synchronously interrupting the light to the CCD camera at the frequency Δf. This steady state signal is integrated over many periods on the CCD ("boxcar" method of measurement [29,50]) until sufficient counts have been collected to provide a good SNR. The steady state amplitude corresponding to a particular phase setting of the Δf signal is obtained by applying a synchronous gate to the cathode of the MCP intensifier, or alternatively by synchronously interrupting the excitation light. The latter method has the advantage that the sample is not illuminated when the fluorescence is not being measured, thereby minimizing photo-decomposition. A series of images is recorded by gating the fluorescence signal at different time delays within the Δf heterodyne cycle. The mode of operation is depicted graphically in Fig. 3. The phase and modulation of the fluorescence sample are deter-

mined simultaneously over the entire image at every pixel from this series of images. The overall fluorescence lifetime is determined relative to the phase delay of a known fluorescence sample or scattering of the excitation light. Details of the instrumentation and experimental procedures will be published separately (R.M. Clegg et al., in preparation).

To apply the homodyne method ($\Delta f = 0$), the phase delay of the MCP modulation must be

applied at the high frequencies of light modulation, f_A. The emission falling on the CCD camera is not interrupted synchronously, but rather accumulated over the entire period (f_A^{-1}). The measurement and data analysis are otherwise essentially identical to those in the heterodyne method. The homodyne technique has been implemented by others [39], and by us (unpublished). The data presented in this paper have been acquired only with the heterodyne method.

3.4. Data analysis to determine the phase and modulation values

Any repetitive time varying function can be expressed as a Fourier series based on the fundamental repetition frequency [51]. Thus, it is not necessary that the excitation light be a single component sinusoidal function, although the analysis is simplified if this is the case; in fact, the AOMs produce almost perfect sine waves [29]. The goal of the analysis is to determine the phase and the modulation amplitude for the fundamental frequency of the recorded signal at every pixel of interest. Even a small image, e.g. consisting of a 100 × 100 array, poses a challenging problem in data analysis. Thus, one seeks to determine the phases and amplitudes with analysis methods that are as rapid as possible yet provide the required accuracy.

Two programs (SINUS, SINUS2L) (T.W.J. Gadella, Jr. et al., in preparation) were written in Fortran to fit the phase images to eqs. (4 and 5). A linear regression is made to the cos $\Phi \cdot$ sin $\Delta\omega t$ and sin $\Phi \cdot$ cos $\Delta\omega t$ terms obtained by expansion of the function sin($\Delta\omega t - \Phi$) [41]. The phase (eq. 6a), modulation (eq. 6b) for each pixel in the image are calculated, yielding the two classical global lifetimes.

$$\tau_\Phi = \frac{1}{\omega}\tan(\Delta\Phi) \tag{7a}$$

$$\tau_M = \frac{1}{\omega}\sqrt{\frac{1}{M^2} - 1} \tag{7b}$$

If the fluorescence of the specimen contains only one lifetime component ($K = 1$ in eq. 3), the
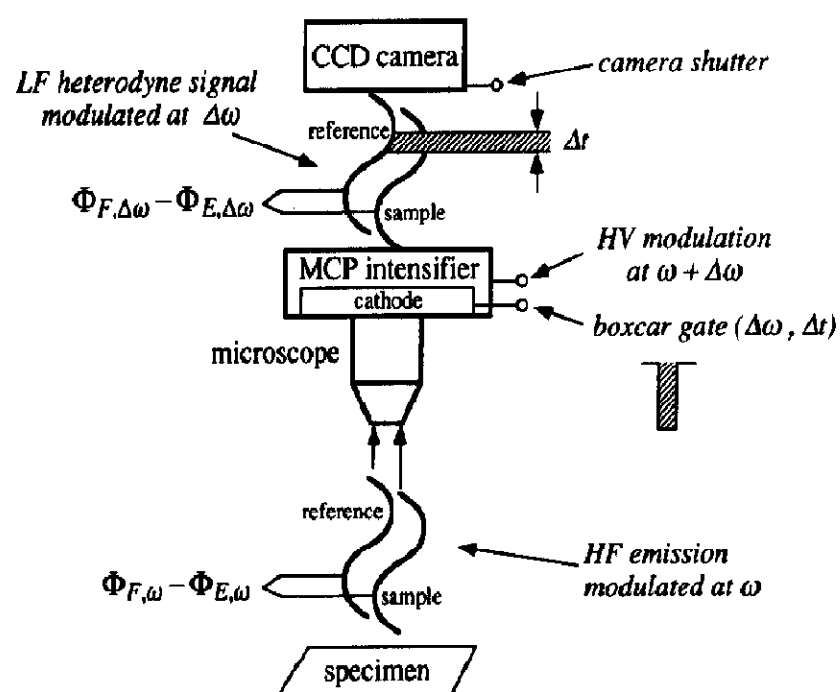

Fig. 2. A schematic of the progression of the optical signal from the fluorescent specimen through the modulated intensifier and to the image-recording CCD camera. The fluorescence emission is modulated at a high frequency ω (radial frequency $\omega = 2\pi f_A$, see text). Modulating the high voltage (HV) amplification of the MCP intensifier at a frequency $\omega + \Delta\omega$ transforms the HF fluorescence signal to a low frequency (LF) component modulated at $\Delta\omega$. The phase delay of the fluorescence relative to the excitation (scattering) is preserved by this heterodyne operation (i.e., $\Phi_{F,\Delta\omega} - \Phi_{E,\Delta\omega} = \Phi_{F,\omega} - \Phi_{E,\omega}$) and the relative modulation is also unchanged (see text). The "reference" compound in the figure refers to light scattering or the emission of a very fast decaying fluorophore; more generally, the reference can be derived from any fluorescence compound with a known lifetime. The phase of the LF sinusoidal signal impinging on every pixel of the CCD camera after being optically relayed from the output phosphor of the MCP, is determined by gating the cathode of the intensifier "on" for a time Δt repetitively and synchronously with the $\Delta\omega$ frequency master. This effects a boxcar detection operation. Separate images are recorded and accumulated on the CCD sensor for a total active observation time = $N\Delta t$, where N = the number of periods averaged for every image and is determined by the total "open" time of the camera shutter, i.e. $N 2\pi(\Delta\omega)^{-1}$. Several phase delay settings are selected by systematically delaying the position of the Δt gate. The images are analyzed as described in the text.

lifetimes obtained from eqs. (7a,b) are identical and equal to the single unique lifetime. In a multicomponent system ($K > 1$ in eq. 3) the lifetimes determined from eqs. (7a,b) will differ such that $\tau_\Phi < \tau_M$. The program SINUS calculates both τ_Φ and τ_M and the standard deviations for each pixel in the image. The program SINUS2L assumes two lifetime components ($K = 2$ in eq. 3) and calculates a second lifetime (τ_2) and a corresponding fractional contribution (α_2) for every pixel provided that one lifetime (τ_1) is known. Both programs perform extensive statistical analyses of the data. They are described elsewhere in detail (T.W.J. Gadella, Jr. et al., in preparation).

It is necessary to perform measurements at several modulation frequencies (f_A) to accurately determine several distinct lifetimes and their fractional contributions in a heterogeneous system. The requirement for gathering large numbers of images that are spatially and photophysically identical and the increase in computation time for analyzing series of data acquired at several frequencies place severe constraints on the systems that can be studied, at least with present technology. For instance, a triple exponential decay yields three lifetime images, three fractional contribution images (which may be reduced to two if one normalizes to 100%) and a steady state fluorescence image. Hence, several phase series of images have to be acquired at different frequencies, the multiple frequency data must be analyzed at every pixel, and six to seven final images have to be considered concurrently in order to assess the spatial distribution of the various lifetime components in the specimen of interest. We would emphasize, however, that the images of τ_Φ and τ_M can be determined accurately and rapidly in all instances, and the analysis is model independent. They provide a valuable and comprehensive account of the spatial dis-
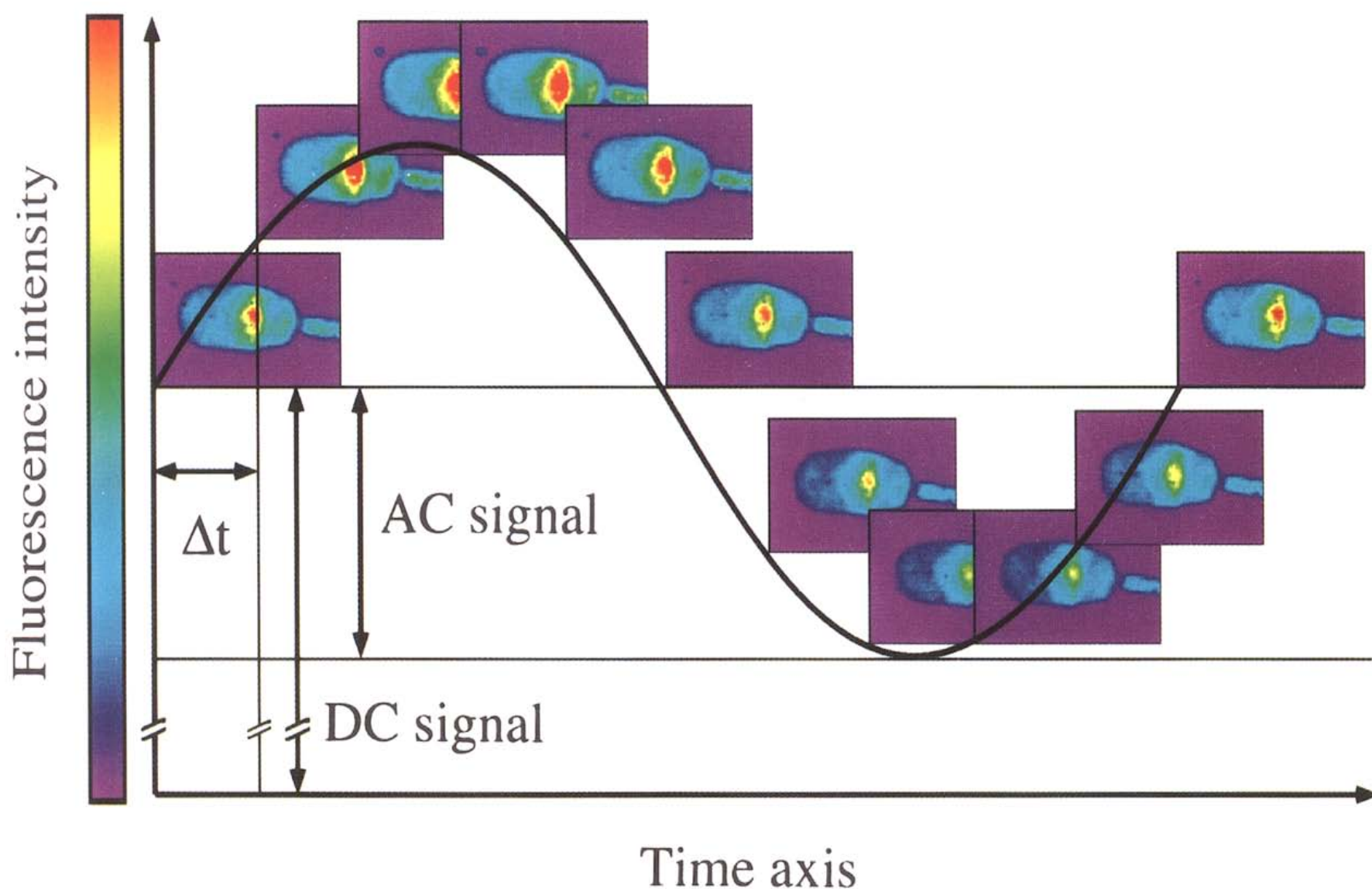

Fig. 3. Typical phase resolved images obtained in FLIM. Experiment as in Fig. 7.

tributed dynamics of fluorescence emission, and reveal immediately whether it is multicomponent in nature.

3.5. Image processing

A significant enhancement to the visual perception of the lifetime data is achieved by image processing (T.W.J. Gadella, Jr. et al., in preparation). The images displayed in the results section were all processed by TCL-Image (TPD, Technical University of Delft; distributed by Multihouse, Amsterdam) and by NIH-Image (National Institutes of Health, Bethesda, MD). Macros were written in TCL-image for calculating one- and two-dimensional histograms displaying the range in temporal distribution of fluorescence lifetimes as well as correlations between lifetimes and fluorescence intensities. This information is combined with images of the original phase dependent data, mathematical reconstructions, difference (original-analysis) intensities, phase and modulation lifetimes, fractional amplitudes, and standard errors into a single output image for display and archiving, as illustrated below.

4. Results and discussion

4.1. Homogeneous samples

A sensitive test of the imaging system is the analysis of a homogeneous sample in which each pixel in the image should display the same fluorescence decay characteristics. The lifetime analyses of rhodamine B in EtOH and a yellow perylene dye embedded in polymethylmethacrylate (PMMA) [1] are shown in Figs. 4 and 5. Table 1 lists the statistical parameters of the fits. The narrow distributions (Fig. 4A) and equivalence
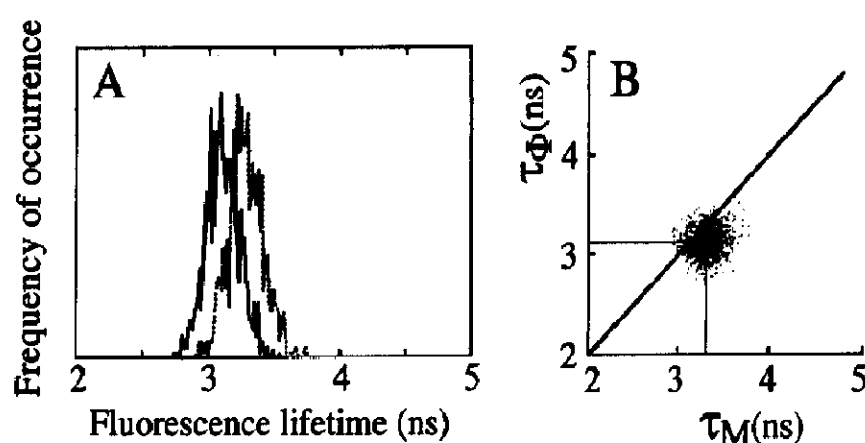
---

[1] Such samples offer many advantages: The plastic pieces can be made very small; they can be machined, and polished after casting. The polymer environment also improves the chemical stability of the dye and minimizes quenching by oxygen. Furthermore, the high emission anisotropies of dyes embedded in PMMA [52] can be exploited.

Fig. 4. Lifetime distribution analysis of rhodamine B in ethanol (~ 1 mg/ml). The sample was placed in a microcuvettte ($h \times w \times l = 0.2 \times 2 \times 50$ mm) from Vitro Dynamics (Rockaway, NJ, USA) and illuminated with the epi-illumination optical system. The 514 nm excitation light, modulated at 39.13 MHz, was reflected from a Zeiss FT 580 dichroic mirror onto the sample. The fluorescence emission passing through a Zeiss LP 590 longpass filter was focused onto the cathode of the MCP intensifier, which was gated on for 2 ms once every 40 Hz heterodyne repetition period (Δf_A^{-1}). Ten images were acquired; the delay of the gate was increased by 2 ms between each consecutive image. The signal for each phase setting was integrated for one second on the CCD camera. (A) distributions of τ_Φ (—) and τ_M (— — —) calculated from $\Delta\Phi$ and M (eq. 7); these parameters were determined from fitting the phase images (each consisting of 800 pixels) to eqs. (5) and (6) using reflected excitation light as reference. (B) two-dimensional histogram depicting the correlation between τ_Φ and τ_M.

(Fig. 4B) of τ_Φ and τ_M for rhodamine B testify to the nearly single component nature of the emission, as expected for this fluorophore [53]. The values of τ_Φ and τ_M at each pixel are uncorrelated, demonstrating that they are independent. For the yellow perylene, $\tau_\Phi < \tau_M$. The implication is that this dye is either in a physical or chemical heterogeneous environment or that its deactivation from the excited singlet state is an inherently multicomponent process ($K > 1$ in eqs. 3a,b). The phase and modulation values (and the corresponding lifetimes) show a narrow distribution, and there are no spatial correlations between τ_Φ and τ_M (Figs. 4B and 5B). These features are indicative of *macroscopic* homogeneity *within* each volume domain encompassed by each pixel (voxel), and of the uniformity of the system response throughout the image. That is, the *microscopic* photophysical heterogeneity at the molecular level is averaged out equally everywhere in the image.

The intensity variations in the original phase images are represented well by sine functions; the correlation coefficient (R) of the fits for both samples is $> 99.5\%$ with an average residual $(res) < 1.2\%$ of the total fluorescence. Of note are the very small average estimated standard error (0.2 ns) and coefficient of variation (CV; 4%) for both τ_Φ and τ_M, showing the repro-

ducibility and precision of the measurement. The histograms of τ_Φ and τ_M have half-widths of ~ 0.3 ns in both cases. By comparing the variance of the lifetimes over the whole image and the average estimated error of each lifetime determination, one can estimate the true spread in the fluorescence lifetimes of the specimen. If n phase images are fit to a sine function [eq. (5)] then the estimated standard error in the lifetime for each pixel $(s_{\tau,i})$ has n-3 degrees of freedom. The observed variance of the mean lifetime for one complete image $(s^2_{\bar\tau,obs})$ is the sum of the "true" or systematic variance of the lifetimes in the specimen $(s^2_{\bar\tau,true})$ and the mean estimated variance in the lifetime determinations of N individual pixels $(\langle s^2_\tau \rangle = (1/N)\Sigma_{i=1}^N s^2_{\tau,i}/(n-3))$.

In principle only $s_{\bar\tau,true}$ is of interest to the experimenter; for the rhodamine sample this quantity is 0.1 ns for τ_Φ and 0.05 ns for τ_M and constitutes a quantitative specification of the homogeneity of the sample and the precision attainable with the instrument. The accuracy of the determination can be assessed by comparison with reference values from the literature (τ of 3.13 ns in this study, obtained at very high concentration, compared to 2.88 ns for more dilute solutions in a cuvette [53]).

Because $\tau_\Phi < \tau_M$ for yellow perylene we know that the fluorescence decay is characterized by more than one lifetime. Assuming a two-component model, it is possible to determine the parameters of a second lifetime component, τ_2 and α_2, if the lifetime of one component is known. In Fig. 5C,D an example is given of this procedure with the data for yellow perylene (see figure legend and Table 1 for details). This routine can be very useful [54], especially for lifetime resolved images. For example, if the total fluorescence signal is comprised of a heterogeneous emission from a single fluorophore, such that only a fraction of the molecules undergo dynamic quenching, one can determine the average quenched lifetime and its fractional contribution if the lifetime of the unquenched probe is known.

These two examples demonstrate the precision and accuracy of the measurement and the use of the technique for accurately determining fluorescence lifetimes in very small volumes < 1 pL.
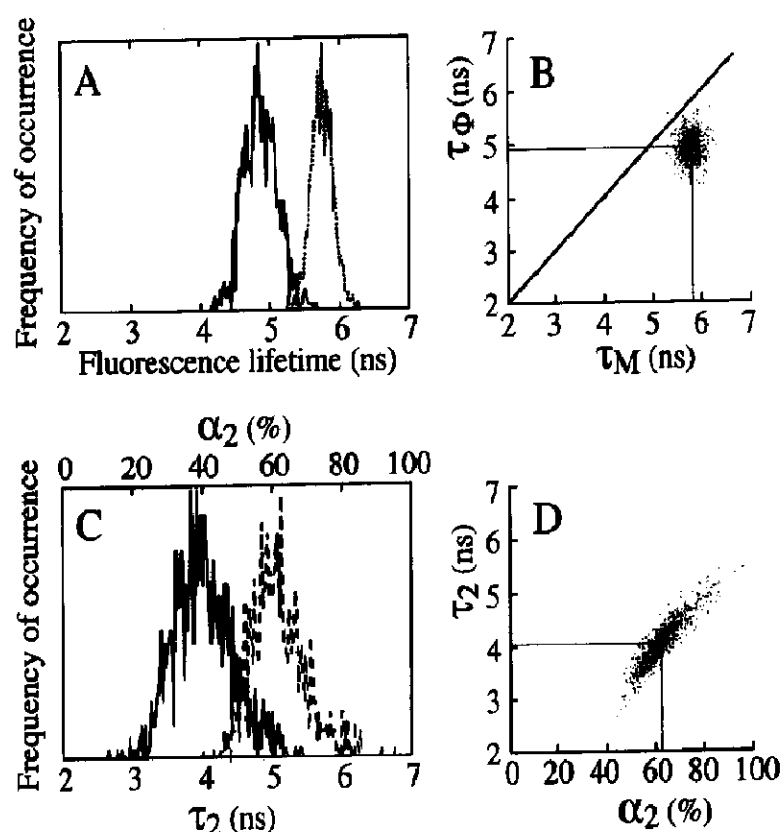

Fig. 5. Lifetime distribution analysis of yellow perylene embedded in plastic. The dye, anthra[2,1,9-d,e,f:6,5,10-d′,e′,f′]diisoquinoline-1,3,8,10(2H,9H)-tetrone-2,9-bis[2,6-bis(1-methylethyl)phenyl], was dissolved in chloroform at ~ 0.1 mg/ml together with 0.5 g/ml polymethylmethacrylate. After evaporation of the chloroform a solid substance was obtained in which the yellow perylene was homogeneously distributed. A tiny piece of this material was mounted on a microscope slide. Excitation was at 488 nm. The fluorescence emission was isolated using a Zeiss FT 505 dichroic mirror and a Zeiss BP 515–565 bandpass filter. The phase images were obtained as described in the legend to Fig. 4. (A) distributions of τ_Φ (—) and τ_M (– – – –) calculated from $\Delta\Phi$ and M (eq. 7) that were determined from fitting the phase images (each consisting of 800 pixels) to eqs. (5) and (6) using scattered light as reference. (B) two-dimensional histogram depicting the correlation between τ_Φ and τ_M. (C) and (D) summarized results of a two-component analysis. One lifetime (τ_1) was arbitrarily set to 10 ns, and the second lifetime (τ_2) and its fractional contribution (α_2) was obtained by substitution of τ_1, and the experimentally derived $\Delta\Phi$ and M into eqs. (3a,b), with $K = 2$ [48,54]. (C) distributions of τ_2 (—) and α_2 (– – – –). (D) correlation between τ_2 and α_2.

4.2. Acridine orange in a 3T3 fibroblast

A fluorescence lifetime image analysis of a mouse fibroblast 3T3 cell labeled with acridine orange (AO) is shown in Fig. 6. The layout of the data and analysis is a general, convenient mode of representation developed in conjunction with the programs SINUS and SINUS2L. It is necessary to display a comprehensive overview due to the large amount of information inherent in lifetime resolved images. The description of the columns of images (from top to bottom) is as follows. The first column shows one of the original images at a particular phase setting, a calculated image representing the amplitude of the time-varying fraction of eq. (5) ($F_{t,\Delta\omega} = F_{0,\Delta\omega} \cdot M_{F,\Delta\omega}$), and a similar calculated image of the static fluorescence signal $F_{0,\Delta\omega}$ at every pixel. The pixels for which the fluorescence intensity was below a preset threshold value are marked with green; these pixels were excluded from the analysis and the statistical evaluation. The second column depicts the calculated τ_Φ and τ_M images, and the computed phase ($\Delta\Phi$) and modulation (M) images. The values of the corresponding fit parameters are displayed according to the accompanying color

tables. Differences in the fluorescence lifetimes at different locations of the cell nucleus exist for both τ_Φ (2–5 ns) and τ_M (3–7 ns). In the third column are the estimated standard error images (estimated from the quality of the fits). The fourth and fifth columns are several one- and two-dimensional histograms showing the temporal distribution, intensity distribution (steady state) and correlations between the fit parameters (such as presented for other samples in Figs. 4 and 5). There is no obvious correlation between the fluorescence lifetimes and intensities (top two histograms in the fifth column). However, the relationship is not completely random; there are areas in Fig. 6, for instance in the nucleoli, where the lifetime and intensity values are correlated. The global statistics attest to the high quality of the image data; the correlation coefficient was 98.4% and the total residuals for the fit were only 2.5% of the measured intensities. The lifetimes were determined with standard errors of 0.2–0.5 ns. The overall lifetime in this case (averaged over the whole image) is less meaningful than for a homogeneous sample; the coefficient of variation was 13% compared to 3% for the rhodamine B solution (Fig. 4).

Table 1

Statistical parameters of the lifetime images [a]

Fluorophore	τ_Φ (ns)	CV (%)	$\langle s_{\tau,i} \rangle$ [b] (ns)	$s_{\bar{\tau},\text{true}}$ (ns)	τ_M (ns)	CV (%)	$\langle s_{\tau,i} \rangle$ (ns)	$s_{\bar{\tau},\text{true}}$ (ns)	R (%)	res (%)
Rhodamine B [c]	3.13	4.0	0.20	0.10	3.31	3.7	0.21	0.05	99.7	1.2
Yellow perylene [d]	4.91	5.0	0.49	0.16	5.80	2.8	0.33	0.11	99.5	1.1
τ_2 [e]	4.04	11	0.89	0.27						
α_2 [f]	0.62	13	0.16	0.05						
Acridine orange [g]	3.30	14	0.35	0.44	4.71	13	0.52	0.59	98.4	2.1
Lissamine–rhodamine [h]	2.36	11	0.30	0.23	2.46	16	0.51	0.33	98.9	2.5

[a] The parameters are defined in the text. The measurements were at ambient temperature.
[b] $\langle s_{\tau,i} \rangle = (1/N)\Sigma_{i=1}^N s_{\tau,i}$.
[c] ~1 mg/ml solution in EtOH.
[d] The kind gift of K. Lieberman, Hebrew Univ., Jerusalem. The dye was codissolved with polymethylmethacrylate in $CHCl_3$ and deposited on a slide.
[e] Second lifetime in a two component analysis, with τ_1 fixed at 10 ns.
[f] The values (except for CV) are dimensionless.
[g] Dye added to fixed 3T3 fibroblasts.
[h] Dye conjugated to sphingolipid used to stain boar sperm.

4.3. Boar sperm labeled with lissamine–rhodamine conjugated to sphingolipids

The lifetime analysis of a boar sperm cell stained with lissamine–rhodamine labeled sphingolipids is shown in Fig. 7 (B.M. Gadella et al., in preparation). The display of the data and analysis are analogous to those in Fig. 6. Despite the large variations in fluorescence intensity the histograms of τ_Φ and τ_M are narrow, and $\tau_\Phi \approx \tau_M$, indicating that the emission was homogenous. The extreme narrow temporal distribution of the lissamine–rhodamine fluorescence lifetime in this specimen is also demonstrated by the fact that $s_{\bar{\tau},\text{true}} < \langle s_{\tau,i} \rangle$ (Table 1). That is, the spread in the temporal histograms (top two images of the fourth column in Fig. 7) was determined mainly by the error associated with the fit. The lack of correlation between fluorescence intensity and lifetime is evident from the two-dimensional histograms for τ_Φ and τ_M (top two images of the fifth column).

The lifetime image analysis is useful for checking the relationship between the fluorescence intensity and the local concentration of the fluorophore (label) in the sample. The steady state fluorescence intensity is proportional to the product of the local concentration and the quantum yield of the fluorophore. In general, for a fluorophore with a single lifetime the quantum yield is proportional to τ (barring static interactions between the dye and other molecules that may affect the apparent quantum yield). The quantum yield cannot be ascertained with the usual steady state measurement in a microscope because the local quantity (concentration [2]) is not known. However, by measuring the fluorescence lifetime, one can determine the amount by which the fluorescence intensity has been reduced due to

dynamic quenching. Figure 8 shows a profile of the fluorescence lifetimes vs. the fluorescence intensities from the data along the yellow line in Fig. 7. It is clear that the fluorescence lifetimes remained constant although the fluorescence intensities varied considerably. As expected the noise in the lifetime profiles is less in the regions of high fluorescence intensity due to better counting statistics in these regions. Because of the constancy of τ in this sample, the intensity profile may be interpreted as a concentration profile. More generally, the lifetime information in images can be used to correct the apparent fluorescence intensities for dynamic quenching on a pixel-by-pixel basis in order to furnish true displays of concentration throughout the image [3]. This important application should be of great use in quantitative cellular fluorescence studies monitoring the distributions of specific labels.

Figure 7 exemplifies the manner in which FLIM can fully exploit the spatial resolution of the optical microscope. A boar sperm cell head has a maximal cross-section of $\sim 0.5 \times 4$ μm and a length of 8 μm, encompassing a volume of only ~ 8 fL (8×10^{-15} L). Nonetheless, a sufficient number of pixels, each of which yields an independent overall lifetime measurement, is available for generating lifetime images of the structure.

4.4. Lifetime suppressed images of intrinsic fluorescence of plant cells

In Fig. 9, another type of analysis is demonstrated for a (living) moss plant *Neckera complanata (Hedw.) Hüb*. The chloroplasts and the carotenoids outside the chloroplasts (near the cell wall) have a predominantly red and green fluorescence, respectively. The chloroplasts (round spots) exhibit a greater red fluorescence intensity than the carotenoids (Fig. 9A,B). The lifetimes of the chlorophylls are expected to vary over an extended range of 10^{-12}–10^{-8} s [56]. The spread of lifetime components can be visualized conve-

---

[2] It is difficult to measure concentrations unambiguously in the microscope due to the use (in general) of optically thin samples and the characteristics of the excitation and detection optical system(s). Out-of-focus contributions can be important in confocal as well as conventional (nonconfocal) systems. One approach is to interpret the apparent concentration as a quantity proportional to the equivalent number of fluorophores in a volume element of the sample corresponding to a pixel (voxel) of the image.

[3] Another method is based on the dynamics of photobleaching at high excitation irradiance [55].
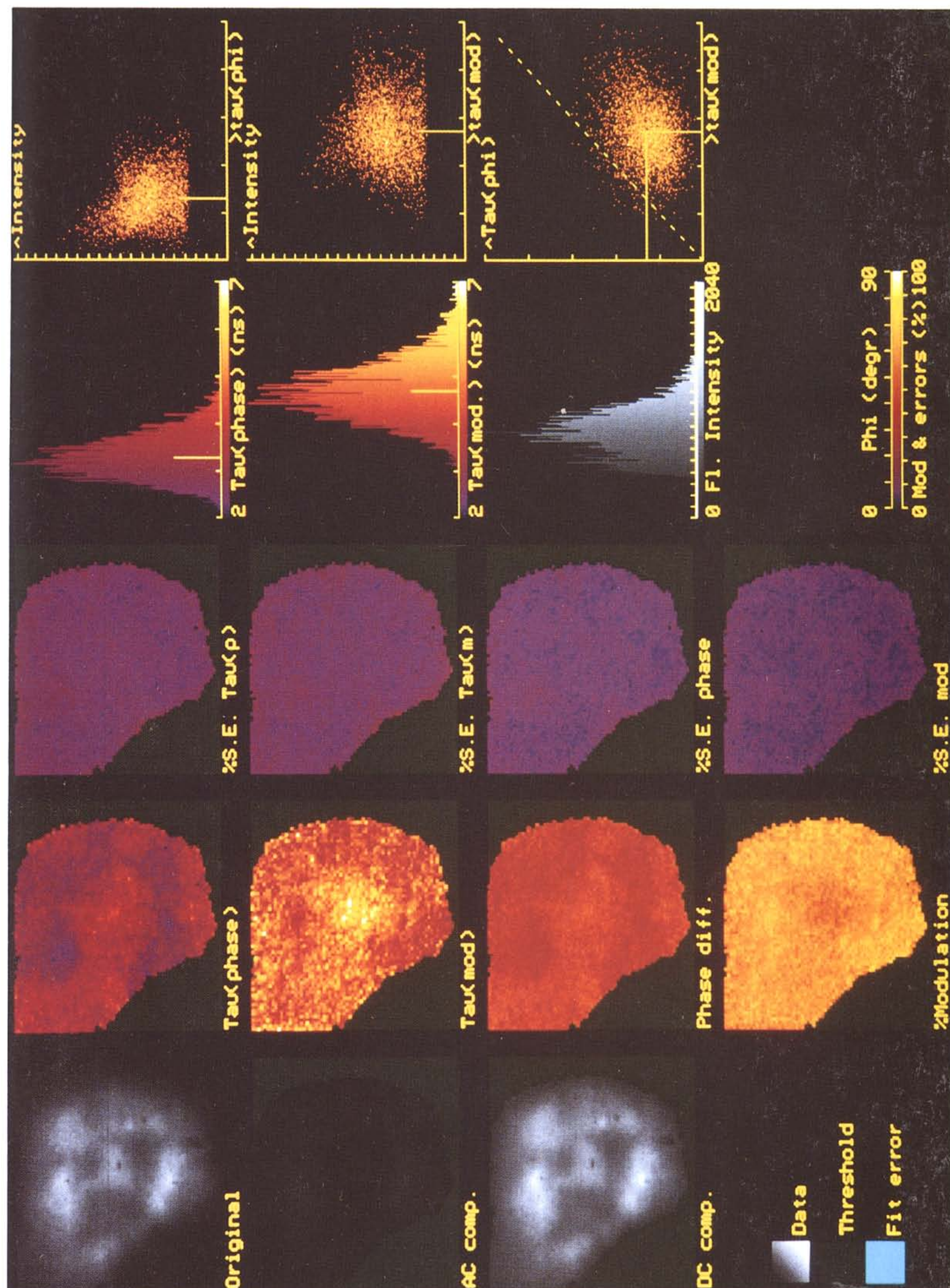
niently by selectively suppressing fluorescence components with particular lifetimes (i.e., with a particular phase delay). This is easily accomplished by subtracting two images taken at phase settings 180° (π radians) apart, as shown in Fig. 9C,D. [4] The intensities in the difference images in Fig. 9C,D at pixels with overall lifetimes shorter (smaller phase delay) than the suppressed lifetime are positive, and those with longer lifetimes (larger phase delays) than the suppressed lifetime are negative. The wide distribution of lifetimes in the leaves of the moss plant is apparent from the large positive and negative intensity excursions in the phase suppression image. This result is in dramatic contrast to the constant lifetime images of the labeled boar sperm (Fig. 8). The physical and chemical origins of this lifetime dispersion are most probably related to the multiplicity of fluorophores and to differences in the developmental, biological and chemical states of the chloroplasts. FLIM should assist in localizing and analyzing critical aspects of the photochemical reactions and photophysical processes related to photosynthesis in living plants. There are many other potential applications related to the photochemistry within subcellular domains of uni- and multi-cellular living organisms.
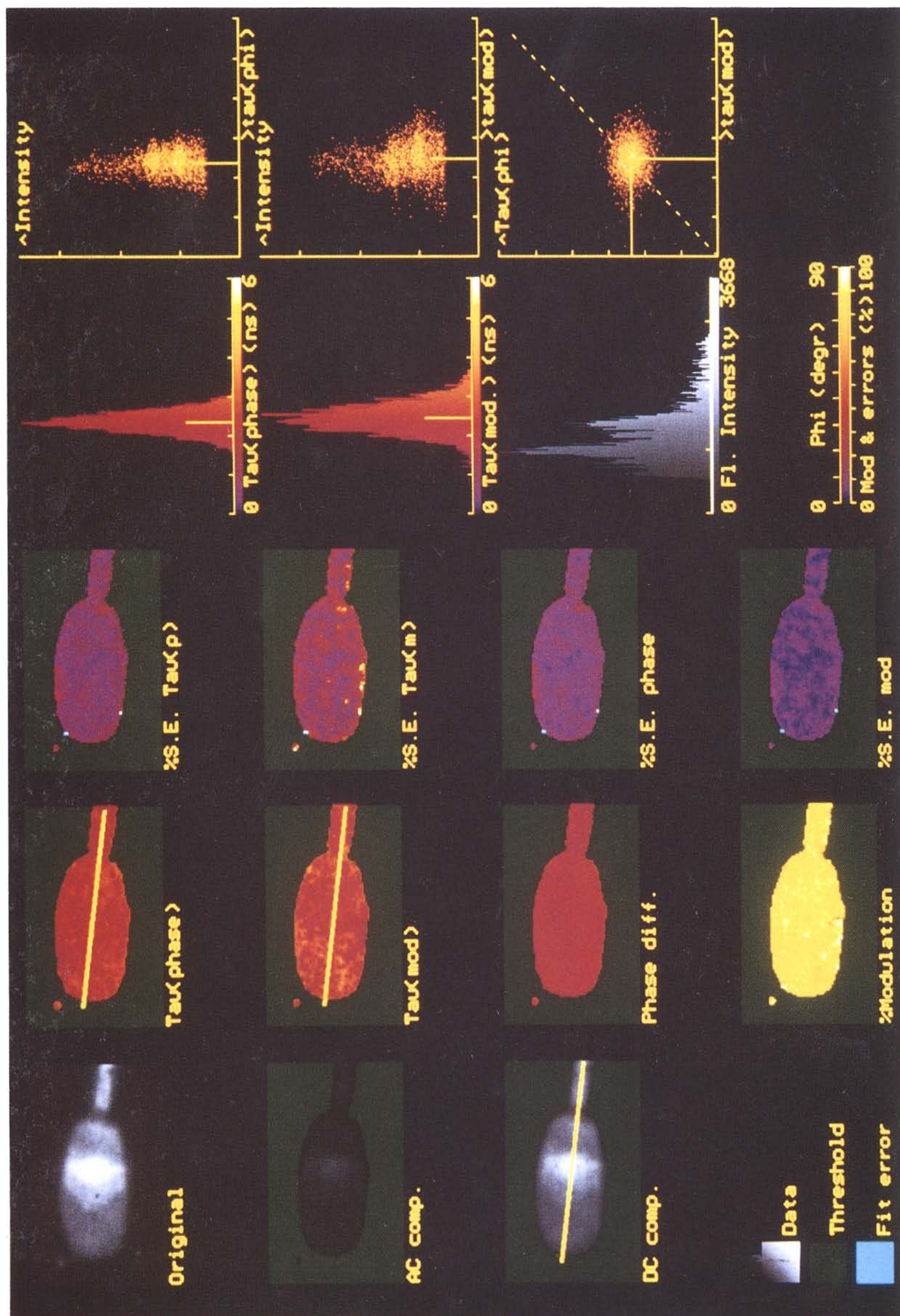
---

[4] It is not necessary that the two images used for selective suppression have a phase differences of π. Any two phase settings ϕ_1 and ϕ_2 (corresponding to $\Delta\omega t_1$ and $\Delta\omega t_2$) suffice, for which the intensities of fluorescence components with a particular lifetime (i.e., phase lag Φ) are equal. The general condition, derived from the identity $\sin\theta = \sin(\pi - \theta)$, is $\phi_2 = (\pi + 2\Phi - \phi_1)$, However, the largest difference amplitudes and thus greatest sensitivity for desired signals with phase lags $\neq \Phi$, is achieved for $\phi_1 = \Phi$ and $\phi_2 = \pi + \Phi$, corresponding to zero crossings of the suppressed component(s).

5. Conclusions

We have demonstrated the applicability of lifetime-resolved prompt fluorescence imaging in the microscope. Incorporating the nanosecond time response directly into the imaging measurement opens up many new possibilities for better defining the molecular state and environment of a fluorophore in the complex environment of a biological system. The fluorescence signal can be decomposed and expanded on the lifetime axis, permitting the resolution of a fluorescence signal into components originating from several species with different lifetimes or of distinct molecular environments of a single fluorophore. The dynamic features of fluorescence can also be combined with other spectroscopic parameters, for example the spectral dependence and polarization of excitation and emission, and fluorescence resonance energy transfer (FRET) between donor and acceptor molecules in close spatial proximity. A comparison of FLIM and conventional fluorescence spectroscopy is given in Table 2. It is seen that the objectives of FLIM measurements are often different from those of cuvette based measurements (see other articles in this issue). The spatial distribution of fluorophores is of prime importance in imaging experiments. The overall spectroscopic parameters that aid in determining the distribution of a particular molecular structure within a larger organized subcellular structure, and the differences (as opposed to the actual values) of the spectroscopic parameters in the different regions of the object, become a major concern, as reflected in the type of data analysis, the presentation of the results (Figs. 4–9), and the correlation of the statistical parameters.

Fig. 6. Lifetime image analysis of acridine orange (AO) fluorescence in a cell nucleus of a mouse fibroblast 3T3 cell stained with AO. The cells were grown on glass coverslips, fixed with methanol and stained with AO as previously described [32]. λ_{ex} was 488 nm. The reference was scattered light. A ×100 NA 1.3 oil immersion objective was used. The frequencies and the filters used were identical to those of Fig. 5. Twenty images were recorded with phase delay settings as described in Fig. 4; however, the phase delay was increased by 2 ms between each consecutive image for the first 10 images, then decreased from 18 to 0 ms in 2-ms steps for the last 10 images. This was done to enable a photobleach correction prior to fitting the data. The correction for every pixel was implemented by adding the digital image intensities corresponding to identical gate delays for both the increasing and decreasing portions of the image series. A comparison of the last and first images (both with 0 ms delay) showed that on the average 10% of the AO molecules were photobleached during the data collection. The figure consists of 5 columns; for a detailed explanation of the data layout see the text.

T.W.J. Gadella Jr. et al. / Biophys. Chem. 48 (1993) 221–239
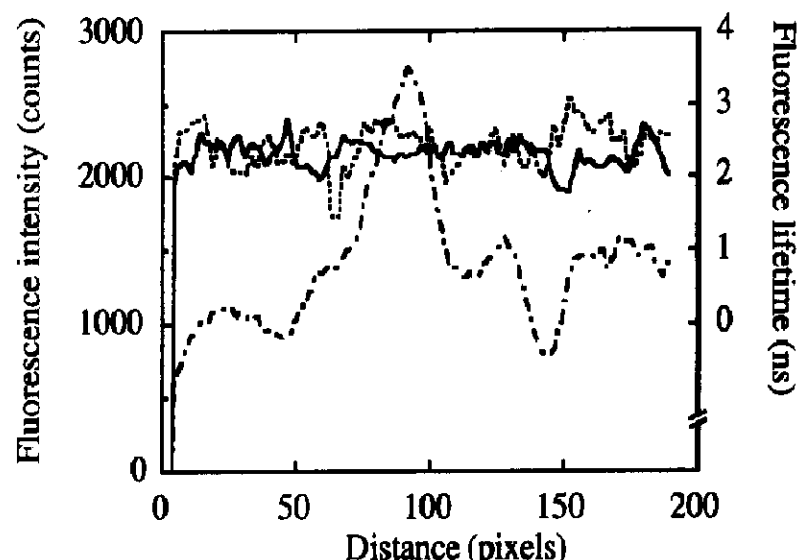
233

Fig. 8. Profile plots of lifetimes and steady state fluorescence in a sperm cell along the yellow lines indicated in Fig. 7. (---), fluorescence intensity; (—), τ_ϕ; (— — —), τ_M.

It has been stressed often in the fluorescence literature that the emission from an excited state of a molecule is a complex process and that steady state measurements are insufficient for the identification of the photophysical processes active in particular situations. Certainly, one's understanding of any fluorescence determination is incomplete without a direct measure of the dynamic characteristics. The lack of direct temporal information can lead to erroneous interpretations of the fluorescence measurement. The complexities accompanying the emission of a single fluorophore in a pure homogeneous solvent are compounded by the introduction of the fluorescence probe into biological systems consisting of multiple macromolecules at high concentration. In this paper we have stressed the utility of lifetime determinations in enabling the quantitative interpretation of fluorescence measurements under such conditions.

In addition to the direct determination of fluorescence lifetimes at every locality of an image simultaneously, FLIM furnishes many other benefits. Phase suppressed images can be acquired and processed rapidly resulting in a valuable qualitative visual representation of the relative lifetime distribution in an image, as well as suppressing undesired fluorescence with a particular lifetime. The discrimination from other fluorescing and scattering components with different lifetimes is possible even if their emission frequencies strongly overlap. Given an appropriate selection of fluorophore for extrinsic labeling, autofluorescence components that often limit the attainable sensitivity of conventional measurements can be suppressed.

The potential and actual sensitivity of lifetime-resolved imaging is suprisingly high, as demonstrated in other experiments conducted in our laboratory with A431 human epidermoid carcinoma cells labeled with dye-conjugated epidermal growth factor (EGF) bound to its cell surface receptor (T.W.J. Gadella Jr. and T.M. Jovin, in preparation). One cell expresses $\sim 10^6$ receptor molecules distributed over the plasma membrane. We have obtained 100×100 pixel images from such cells, such that one pixel comprises on average the fluorescence from only 10 molecules.

An alternative to the phase and modulation technique that operates in the frequency domain, is to measure images directly in the time domain using pulsed excitation light. In principle, identical information is available from both methods. However, because of differences in the instrumentational realization and capabilities of these techniques they are often complementary. The

Fig. 7. Lifetime image analysis of a boar sperm cell stained with a lissamine–rhodamine labeled sphingolipid β-1,1′(N-lissamine rhodaminyl-[12 amino-dodecanoyl])sphingosine (GalCer-Rh), a kind gift of Dr. Marchesini [57], was administered to washed boar spermatozoa [58] using unilamellar vesicles containing 85 mol% egg PC (Sigma), 15 mol% GalCer-Rh [59,60] for 10 min at 37°C. The unfused vesicles were removed by washing the spermatozoa over a 55% Percoll (Pharmacia) gradient. The spermatozoa were immobilized on coverslips coated with zona pellucida matrix (the extracellular matrix of the oocyte; [61]) and mounted in glycerol. The mobility and the integrity of the sperm morphology, specificially of the plasma membrane, was checked according to [58]. λ_{ex} was 488 nm. The filters and the objective were as in Figs. 4 and 6, respectively. The modulation frequency f_A was 39.13 MHz and the difference frequency Δf was 10 Hz. Twenty phase images were collected as described in Fig. 6; however, the open gate time was 9.9 ms and the phase difference between the phase images was 10 ms. A linear photobleach correction was performed prior to fitting of the data (as in Fig. 6); the average amount of photobleaching over the course of the experiment was less than 10%. The layout of the data is as in Fig. 6.

choice between the two methods depends on the type of information desired, and on the fluorescence lifetimes of the luminescence components. It is of interest to compare some of their important characteristics: (i) The phase analysis at each frequency is rapid and accurate and does not involve deconvolution of the signal with the shape of the excitation pulse; the data at one frequency can be used to phase suppress particular components. For the time domain method, if the excitation pulse is not short compared to the fluorescence lifetimes, an accurate analysis of the data cannot be carried out without deconvolution. This can take a long time if the image contains many pixels. (ii) Using time domain imaging, two fluorescence lifetimes that are well separated can be distinguished if the observation can be delayed until the fastest decay has subsided, thereby permitting the sensitive measurement of the slower component without any interference from the fast decay. Using the frequency dispersion method, it is difficult to accurately detect a slower component with a low amplitude in the presence of a much larger, faster component (see eqs. 3a,b). On the other hand, closely spaced lifetime components can be easily separated by phase in the
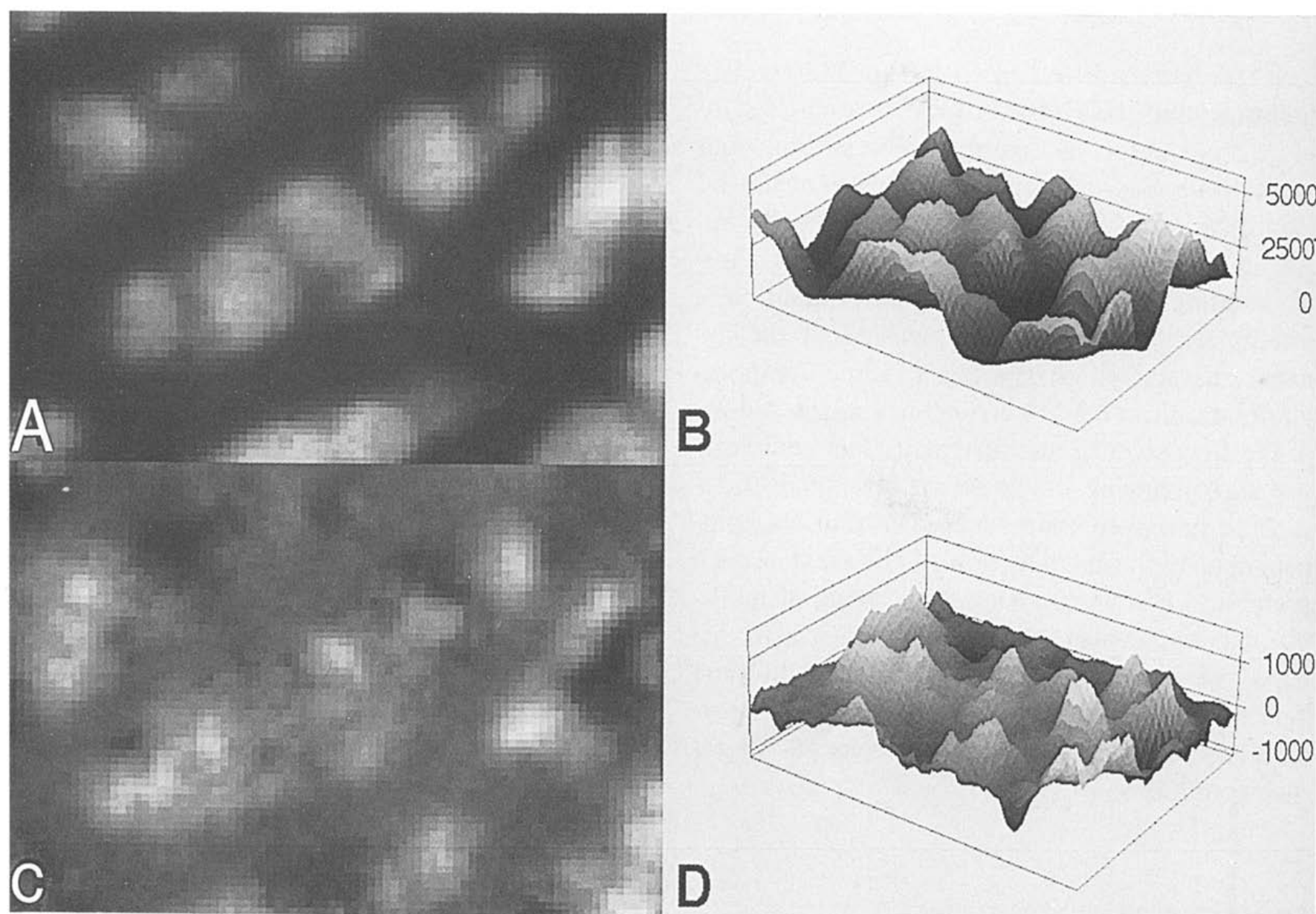

Fig. 9. Phase suppression of the red autofluorescence originating from a moss plant cell. One leaf was removed from a freshly harvested moss plant *Neckera complanata (Hedw.) Hüb.* and mounted in water under a cover slip on a microscope slide. The specimen was prevented from drying by sealing the coverslip to the slide with nail polish. λ_{ex} was 488 nm, and the red fluorescence was imaged using the filters and the objective of Fig. 7. The modulation frequency f_A was 39.13 MHz and the difference frequency Δf was 100 Hz. Phase images were collected as described in Fig. 6; however, the open gate time was 0.99 ms and the phase delay between consecutively acquired images was 1 ms. A linear photobleach correction was made as described in Fig. 6; the extent of photobleaching did not exceed 10% during the experiment. (A) and (B) steady state autofluorescence with a grey scale representation and as a pseudo 3-D grey-scaled image. The field is 75×120 pixels. (C) and (D) results of phase suppressing particular lifetimes; the phase suppression was performed by subtracting the corrected intensities of the two images collected with gated time delays of 1 and 6 ms.

Table 2

Comparison of time resolved fluorescence spectroscopy and fluorescence lifetime imaging microscopy (FLIM)

Time resolved fluorescence spectroscopy	Fluorescence lifetime imaging microscopy (FLIM)
Accurate multiple lifetimes or lifetime distribution of purified compounds	Accurate spatial distribution of average lifetimes of a mixture of compounds in a natural cellular milieu
Many modulation frequencies	Generally a *single* frequency
Single spot excitation: one cuvette at a time	Whole image excited simultaneously: typically 10^3–10^5 pixels (voxels or minicuvettes)
Long computation times per cuvette are allowed	A lifetime fit for one pixel requires a few ms
Multiple cells	Single cells or subcellular compartments
Comparison of fluorescence lifetimes or lifetime distribution with other cuvette experiments (as a function of other physical parameters)	Comparison of spatial fluorescence lifetime distribution with fluorescence intensity distribution; colocalization with other fluorescent dyes and/or correlation with phase contrast image
Lifetimes are varied *by the experimentor* by modifying the (physical or chemical) conditions in the cuvette	Lifetimes differ in an image due to differential conditions inside cellular compartments, generally *beyond* the control of the experimentor

frequency domain; this is generally difficult to achieve in the time domain. (iii) At present, the frequency method allows shorter lifetimes to be determined from two-dimensional images acquired with an MCP intensifier. With streak cameras, the time response of the pulse-time method has been extended into the picosecond region [31]; however, only one-dimensional time resolved images can be acquired simultaneously, and the second dimension must be scanned. (iv) The substantial energy and very short excitation pulses required for the time domain technique leads to a requirement for elaborate arc lamp (pulsed) or laser (pulse, Q-switched, mode-locked) excitation sources. In contrast, any CW laser with the appropriate wavelength can be used with the frequency method, and exceptionally large light intensities are not required. Circuits for modulating lamps at high frequencies (up to 30 MHz) have been reported [44]; these would be convenient as broadband light sources for frequency domain imaging.

We conclude by emphasizing that FLIM is a relatively new technique, but it should not be considered as an experimental method that will be available only in the future, or exist only in a few instrumentationally orientated laboratories.

The phase-and-modulation lifetime-resolved imaging microscope we have described is a stable, robust laboratory instrument that is convenient and simple to use. FLIM is available now. However, the development of both the frequency and time domain techniques will be necessary to fully exploit the extensive possibilities of FLIM. We hope that the FLIM will be implemented by many research groups, and that it will be applied routinely as a useful extension in laboratories presently using steady state fluorescence microscopy. In addition to its utility as a research tool, a number of important biomedical and analytical applications for FLIM can be anticipated.

and 8). We thank Dr. Marchesini (University of Brescia, Italy) for providing the lissamine-rhodamine-labelled galactoceramide, and K. Liebermann (Hebrew University, Jerusalem) for providing the yellow perylene. We are grateful to B.F. Clegg for continuously providing fresh moss plants, and to Dr. T.W.J. Gadella, Sr. (University of Utrecht) for their identification.

References

1 B. Herman and K. Jacobson, eds., Optical microscopy for biology (Wiley–Liss, New York, 1990).

2 R.P. Haugland, in: Optical microscopy for biology, eds. B. Herman and K. Jacobson (Wiley–Liss, New York, 1990) pp. 143–157.

3 R.Y. Tsien, Meth. Cell Biol. 30 (1989) 127–156.

4 R.Y. Tsien and A. Waggoner, in: Confocal microscopy handbook, ed. J.B. Pawley (Plenum Press, New York, 1990) pp. 169–178.

5 L.M. Loew, D.L. Parkas and M.-D. Wei, in: Optical microscopy for biology, eds. B. Herman and K. Jacobson (Wiley–Liss, New York, 1990) pp. 131–142.

6 R.P. Haugland, Molecular probes: handbook of fluorescent probes and research chemicals, 5th edn. (Molecular Probes, Eugene, OR, 1992).

7 D.L. Taylor and Y.L. Wang, eds., Fluorescence microscopy of living cells in culture, part A. Fluorescent analogs of peptides and hormones. Meth. Cell Biol. 29 (Academic Press, New York, 1989).

8 R.S. Aikens, D.A. Agard and J.W. Sedat, Meth. Cell Biol. 29 (1989) 291–313.

9 K.R. Spring and P.D. Smith, J. Microsc. 147 (1987) 265–278.

10 G.R. Bright, G.W. Fisher, J. Rogowska and D.L. Taylor, Meth. Cell. Biol. 30 (1989) 157–190.

11 A. Waggoner, R. DeBiasio, P. Conrad, G.R. Bright, L. Ernst, K. Ryan, M. Nederlof and R.D. Taylor, Meth. Cell. Biol. 30 (1989) 449–476.

12 K.A. Giuliano, M.A. Nederlof, R. DeBasasio, L. Frederick, A.S. Waggoner and D.L. Taylor, in Ref. 1, pp. 543–558.

13 E. Ohmes, J. Pauluhn, J.-U. Weidner and H.W. Zimmermann, Ber. Bunsenges. Phys. Chem. 84 (1980) 23–36.

14 J.A. Dix and A.S. Verkman, Biophys. J. 57 (1990) 231–240.

15 K. Florine-Casteel, J.J. Lemasters and B. Herman, in: Optical microscopy for biology, eds. B. Herman and K. Jacobson (Wiley–Liss, New York, 1990) pp. 559–574.

16 T.P. Burghardt and K. Ajtai, in: Topics in fluorescence spectroscopy, vol. 2: Principles, ed. J.R. Lakowicz (Plenum Press, New York, 1991) pp. 307–343.

17 W.E. Mickols, M.F. Maestre, J.I. Tinoco, Jr. and S.H. Embury, Proc. Natl. Acad. Sci. USA 82 (1985) 6527–6531.

18 D.A. Beach, K.S. Wells, F. Husher and C. Bustamante, Rev. Sci. Instrum. 58 (1987) 1987–1995.

19 D.A. Beach, C. Bustamante, K.S. Wells and K.M. Foucar, Biophys. J. 53 (1988) 449–456.

20 M.H. Kim, L. Ulibarri and C. Bustamante, Biophys. J. 52 (1987) 929–946.

21 B. Herman, Meth. Cell Biol. 30 (1989) 219–243.

22 T.M. Jovin and D.J. Arndt-Jovin, in: Cell structure and function by microspectrofluorometry, eds. E. Kohen and J.G. Hirschberg (Academic Press, New York, 1989) pp. 99–117.

23 D.M. Jameson and G.D. Reinhart, eds., Fluorescent biomolecules: methodologies and applications (Plenum Press, New York, 1989).

24 J.R. Lakowicz, ed., Topics in fluorescence spectroscopy, vol. 2: Principles (Plenum Press, New York, 1991).

25 J.R. Lakowicz, ed., Topics in fluorescence spectroscopy, vol. 3: Biochemical applications (Plenum Press, New York, 1991).

26 D.J. Arndt-Jovin, S.A. Latt, G. Striker and T.M. Jovin, J. Histochem. Cytochem. 27 (1979) 87–95.

27 J.A. Dix and A.S. Verkman, Biochemistry 29 (1990) 1949–1953.

28 A.S. Verkman, M. Armijo and K. Fushimi, Biophys. Chem. 40 (1991) 117–125.

29 R.M. Clegg, B. Feddersen, E. Gratton and T.M. Jovin, Proc. SPIE 1604 (1992) 448–460.

30 X.F. Wang, A. Periasamy and B. Herman, Crit. Rev. Anal. Chem. 23 (1992) 369–395.

31 T. Minami and S. Hirayama, J. Photochem. Photobiol., A: Chemistry 53 (1990) 11–21.

32 G. Marriott, R.M. Clegg, D.J. Arndt-Jovin and T.M. Jovin, Biophys. J. 60 (1991) 1374–1387.

33 X.F. Wang, S. Kitajima, T. Uchida, T. Coleman and S. Minami, Appl. Spectrosc. 44 (1990) 25–30.

34 X.F. Wang, T. Uchida, D.M. Coleman and S. Minami, Appl. Spectrosc. 45 (1991) 360–366.

35 L. Seveus, M. Väisälä, S. Syrjänen, M. Sandberg, A. Kuusisto, R. Harju, J. Salo, I. Hemmilä, H. Kojola and E. Soini, Cytometry 13 (1992) 329–338.

36 H.B. Beverloo, A. van Schadewijk, S. van Gelderen-Boele and H.J. Tanke, Cytometry 11 (1990) 561–570.

37 E.P. Buurman, R. Sanders, A. Draauer, H.C. Gerritsen, J.J.F. van Deen, P.M. Houpt and Y.K. Levine, Scanning 14 (1992) 155–159.

38 E. Gratton, B. Feddersen and M. van de Ven, Proc. SPIE 1204 (1990) 21–25.

39 J.R. Lakowicz and K.W. Berndt, Rev. Sci. Instrum. 62 (1991) 1727–1734.

40 J.R. Lakowicz, Laser Focus World May (1992) 60–80.

41 J.R. Lakowicz, H.S. Szmacinski, K. Nowaczyk, K.W. Berndt and M. Johnson, Anal. Biochem. 202 (1992) 316–330.

42 J.R. Lakowicz, H.S. Szmacinski and K. Nowaczyk, Proc. Natl. Acad. Sci. (USA) 89 (1992) 1271–1275.

43 D.W. Piston, D.R. Sandison and W.W. Webb, Proc. SPIE 1604 (1992) 379–389.

T.W.J. Gadella Jr. et al. / Biophys. Chem. 48 (1993) 221–239

239

44 C.G. Morgan, A.C. Mitchell and J.G. Murray, J. Microscopy 165 (1992) 49–60.

45 T. French, E. Gratton and J. Maier, Proc. SPIE 1604 (1992) 254–261.

46 R.D. Spencer and G. Weber, Ann. N.Y. Acad. Sci. 158 (1969) 361–376.

47 R.B. Cundall and R.B. Dale, eds., Time-resolved fluorescence spectroscopy in biochemistry and biology (Plenum Press, New York, 1983).

48 D.M. Jameson, E. Gratton and R.D. Hall, Appl. Spectrosc. Rev. 20 (1984) 55–106.

49 D.W. Piston, G. Marriott, T. Radivoyevich, R.M. Clegg, T.M. Jovin and E. Gratton, Rev. Sci. Instrum. 60 (1989) 2596–2600.

50 R.M. Clegg, G. Marriott, B.A. Feddersen, E. Gratton and T.M. Jovin, Biophys. J. 57 (1990) 375a.

51 S. Goldman, Frequency analysis, modulation and noise (Dover, New York, 1948).

52 A.F. Corin, E. Blatt and T.M. Jovin, Biochemistry 26 (1987) 2207–2217.

53 R.A. Lampert, L.A. Chewter, D. Phillips, D.V. O'Conner,

A.J. Roberts and S.R. Meech, Anal. Chem. 55 (1983) 68–73.

54 G. Weber, J. Phys. Chem. 85 (1981) 949–953.

55 T.M. Jovin, D.J. Arndt-Jovin, G. Marriott, R.M. Clegg, M. Robert-Nicoud and T. Schormann, in: Optical Microscopy for Biology, eds. B. Herman and K. Jacobson, (Wiley–Liss, New York, 1990) pp. 575–602.

56 M. Werst, Y. Jia, L. Mets and G.R. Fleming, Biophys. J. 61 (1992) 868–878.

57 S. Marchesini, A. Preti, M.F. Aleo, A. Casella, A. Dagan and S. Gatt, Chem. Phys. Lipids 53 (1990) 165–175.

58 B.M. Gadella, B. Colenbrander, L.M.G. Van Golde and M. Lopes-Cardozo, Biochim. Biophys. Acta 1128 (1992) 155–162.

59 J.P. Vos, M.L. Giudici, L.M.G. Van Golde, A. Preti, S. Marchesini and M. Lopes-Cardozo, Biochim. Biophys. Acta 1126 (1992) 269–276.

60 N.G. Lipsky and R.E. Pagano, J. Cell Biol. 100 (1985) 27–34.

61 B.S. Nikolajczyk and M.G. O'rand, Biol. Reprod. 46 (1992) 366–372.